Modeling Virtualized Downlink Cellular Networks with Ultra-dense Small cells

Hazem Ibrahim, Hesham ElSawy, Uyen T. Nguyen, and Mohamed-Slim Alouini

Abstract—The unrelenting increase in the mobile users' populations and traffic demand drive cellular network operators to densify their infrastructure. Network densification increases the spatial frequency reuse efficiency while maintaining the signal-to-interference-plus-noise-ratio (SINR) performance, hence, increases the spatial spectral efficiency and improves the overall network performance. However, control signaling in such dense networks consumes considerable bandwidth and limits the densification gain. Radio access network (RAN) virtualization via control plane (C-plane) and user plane (U-plane) splitting has been recently proposed to lighten the control signaling burden and improve the network throughput. In this paper, we present a tractable analytical model for virtualized downlink cellular networks, using tools from stochastic geometry. We then apply the developed modeling framework to obtain design insights for virtualized RANs and quantify associated performance improvement.

Keywords:- RAN virtualization, Phantom Cell, Heterogenous Networks, Stochastic Geometry.

I. INTRODUCTION

The number of mobile users using the cellular infrastructure for Internet connectivity is drastically increasing due to the rapid proliferation of smart phones, tablets, and PDAs with powerful processing capability. This results in increasing traffic demands on cellular networks to support data applications at higher throughputs. It is expected that by 2020 there will be more than 50 billion connected mobile users, and the cellular infrastructure should be developed accordingly [1]. In response to these challenges, cellular operators seek all means for increasing their network capacity and net throughput. Network densification via small cell deployment is an appealing approach as it maintains the signal-to-interference-plus-noise-ratio (SINR) performance while increasing the spatial frequency reuse efficiency [2]. Deploying more small cells decreases the service area of each small base station (SBS) and hence increases the spatial frequency reuse. Furthermore, a smaller cell area leads to a smaller number of associated users per SBS, which increases the per-user throughput. Note that densification via SBS deployment is preferred over densification via macro base station (MBS) deployment due to lower costs and faster deployment.

Increasing the BS density increases the data rate, but also increases the control signaling per unit area. Furthermore, smaller cell areas imply more control signaling, and hence
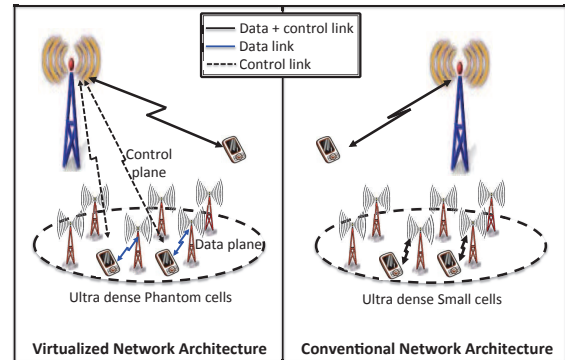

Fig. 1. Virtualized vs. conventional network architectures.

lower data rates, due to higher handover rates. In other words, the control signaling burden may limit the performance gain achieved via densification. Radio access network (RAN) virtualization via control plane (C-plane) and user plane (U-plane) splitting, shown in Fig. 1, has been proposed as a potential solution to mitigate the control signaling burden [3]. In this case, the MBSs handle the control signaling for small cell users, leaving the SBS to transmit only data frames. The small cells in a virtualized RAN are referred to as *Phantom BS* as their identities are hidden from the users[1]. That is, the connection to a Phantom cell is transparent to the users because the cell specific control signals, which identify each BS, are not broadcast. Phantom cell selection and associated control are handled by the MBS, which minimizes the handover signaling burden, thanks to the larger coverage of a macro cell. Moreover, defining the control plane at the macro cell level requires less control overhead [4], which further improves the network throughput. It is worth noting that splitting user and control planes necessitates a corresponding split in the frequencies, to avoid interference between control and user signals, which further improves the SINR performance.

The analysis in this paper is based on stochastic geometry modeling. For the sake of tractability, we assume that the BSs of each tier and users follow independent Poisson point processes (PPP). This assumption is widely accepted and has been proven to give simple yet accurate results for the

[1]Phantom BS will also be abbreviated as SBS.

performance of cellular networks. For instance, the authors of [5]–[7] use the PPP assumption to model the coverage probability and rate in downlink multi-tier cellular networks. The authors of [8], [9] model the coverage probability and rate for uplink cellular networks. Renzo et al. [10] also use PPP to evaluate the performance of MIMO cellular networks.

Simple yet accurate mathematical expressions obtained from stochastic geometry models have helped solving important design problems for cellular networks [11]. For instance, Cao et al. [12] exploit stochastic geometry to develop a capacity extension policy for a two-tier heterogeneous network (Het-Net). Syu and Lee [13] study the feasibility of device-to-device communications, while Lin et al. [14] propose an optimal spectrum partitioning between cellular and device-to-device users. Bai and Heath [15] offer design insights for millimeter wave (mmW) based cellular networks. However, none of existing works has addressed the effect of control signaling and network virtualization. To the best of our knowledge, this work is the first that proposes a tractable analytical paradigm for virtualized RAN in cellular networks.

In this paper, we develop a tractable modeling paradigm for virtualized downlink RAN in a two-tier cellular network with flexible cell association. The model accounts for the signaling overhead in the conventional and virtualized network architectures. However, modeling the effect of handover on the control signaling is postponed to future work. To this end, we quantify the expected performance gain for RAN virtualization, obtain design insights, and discuss the feasibility of C-plane/U-plane splitting.

The remainder of the paper is organized as follows. In Section II, we provide the system model, assumptions, and the methodology of analysis. In Section III, we present the performance analysis for the average coverage probability and average throughput improvement via RAN virtualization. We validate the proposed model and discuss the results in Section IV. Finally, Section V concludes the paper.

II. SYSTEM MODEL AND ASSUMPTION

A. Network Model

We consider a two-tier downlink heterogeneous cellular network (HCN). The locations of the BSs in the kth tier ($k = 1, 2$) are modeled as two dimensional homogeneous Poisson point processes (PPP) Φ_k of density λ_k. The macro tier is denoted by $k = 1$ and small cells (Phantom cells), by $k = 2$. Mobile users are spatially distributed according to independent PPP Φ_u with density $\lambda^{(u)}$. All BSs in the kth tier transmit with the same power P_k and always have packets to transmit. We consider a general power law path loss model for both desired and interference downlink signals from the BSs in tier k where signals are assumed to experience path loss

exponent α_k. Furthermore, signal attenuation due to multi-path fading is modeled using an independent (i.e., from the locations) Rayleigh distribution such that the channel power gain $H_x \sim \exp(1)$.

We consider a flexible BS association criterion in which mobile users select the serving BS using the biased average received signal power. That is, let r_k denote the distance between a typical mobile user and the nearest BS of the kth tier and B be the bias factor. Then the mobile user is served by the macro tier if $P_1 r_1^{-\alpha_1} > P_2 B r_2^{-\alpha_2}$, and by a small/Phantom cell otherwise. The bias factor B artificially encourages/discourages users to associate themselves with a certain tier. Thus by manipulating B, we can divide the traffic between the two network tiers and control the portion of mobile users served by each tier. Based on the aforementioned association criterion, the mobile users are divided into the following non-overlapping disjoint sets:

$$u \in \begin{cases} \boldsymbol{U}_1 & \text{if } P_1 r_1^{-\alpha_1} \geq P_2 B r_2^{-\alpha_2} \\ \boldsymbol{U}_2 & \text{if } P_2 r_2^{-\alpha_2} > P_1 r_1^{-\alpha_1} \\ \boldsymbol{U}_B & \text{if } P_2 r_2^{-\alpha_2} \leq P_1 r_1^{-\alpha_1} < P_2 B r_2^{-\alpha_2} \end{cases} \quad (1)$$

where $\boldsymbol{U}_1$ denotes the set of macro users, $\boldsymbol{U}_2$ denotes the set of small/phantom cell users, $\boldsymbol{U}_B$ is the set of biased small/Phantom cell users (i.e., users who are artificially offloaded from the macro tier by the bias factor), and $\boldsymbol{U}_1 \cup \boldsymbol{U}_2 \cup \boldsymbol{U}_B = \boldsymbol{\Phi}_u$.

B. Spectrum Allocation and Control Burden

In order to conduct a fair comparison, we assume that both networks (i.e., virtualized and conventional) have the same available spectrum (W). We define the average data rate using Shannon's formula as $W \ln(1 + \text{SINR})$.

In the conventional network architecture, we assume universal frequency reuse with no intra-cell interference. We also assume interference management through almost blank subframes (ABS) between macro cells and biased small cells [5]. That is, a fraction η of time is dedicated for serving biased mobile users (i.e., $\boldsymbol{U}_B$) with no interference from the macro tier (i.e., MBSs send only ABS). In the conventional network architecture, each BS delivers the control data and user data to each mobile user. Then, if the control overhead consumes a fraction μ of the delivered data rate, the throughput per BS in each case in the conventional network architecture is

$$\mathcal{T}_1^{(c)} = (1 - \mu)(1 - \eta) W \mathbb{E}[\ln(1 + \text{SINR}_1^{(c)})], \quad (2)$$

$$\mathcal{T}_2^{(c)} = (1 - \mu)(1 - \eta) W \mathbb{E}[\ln(1 + \text{SINR}_2^{(c)})], \quad (3)$$

$$\mathcal{T}_B^{(c)} = (1 - \mu)\eta W \mathbb{E}[\ln(1 + \text{SINR}_B^{(c)})]. \quad (4)$$

In the case of the virtualized network architecture, each network tier has its own dedicated spectrum. That is, in order to alleviate interference between user and control signals, W_1 Hz is assigned to the macro tier and $W_2 = W - W_1$ is assigned to the Phantom cell tier. Since each network tier has its own dedicated spectrum and the control signaling is offloaded to

the macro tier, the average throughput for the small cells (i.e., Phantom cells) becomes:

$$\mathcal{T}_2^{(v)} = W_2(1 - \eta)\mathbb{E}[\ln(1 + \text{SINR}_2^{(v)})], \tag{5}$$

$$\mathcal{T}_B^{(v)} = W_2\eta\mathbb{E}[\ln(1 + \text{SINR}_B^{(v)})], \tag{6}$$

and the macro tier average throughput reduces to:

$$\mathcal{T}_1^{(v)} = (1 - \mu)\left(\mathcal{R}_1^{(v)} - \frac{\lambda_2}{\lambda_1}\frac{\mu\left(\mathcal{T}_2^{(v)} + \mathcal{T}_B^{(v)}\right)}{\gamma}\right), \tag{7}$$

where $\mathcal{R}_1^{(v)} = W_1\mathbb{E}[\ln(1 + \text{SINR}_1^{(v)})]$ is the macro cell data rate, γ is the percentage of control signaling reduction[2], $\frac{\mu\left(\mathcal{T}_2^{(v)} + \mathcal{T}_B^{(v)}\right)}{\gamma}$ is the average control signaling required for each Phantom cell and $\frac{\lambda_2}{\lambda_1}$ is the average number of Phantom cells per macro cell. It is worth noting that, although there is no cross-tier interference in the virtualized network architecture due to spectrum splitting, time sharing still exists in (5) and (6) because the SBSs dedicate a fraction η of time to serve biased users.

C. Methodology of Analysis

This paper focuses on quantifying the average coverage probability and average throughput improvement via RAN virtualization. To obtain mathematical expressions for these performance metrics, first we have to characterize the association probability, the service distance, and BSs' traffic load per tier. The association probability is the probability that a typical user is in any of the three sets $\mathcal{U}_1$, $\mathcal{U}_2$, and $\mathcal{U}_B$. Then, given a user association, the service distance characterizes the distribution of the distance from the mobile user to its serving BS. It is worth noting that characterizing the service distance is very crucial as it affects both the intended signal and the interference protection around the user equipment. Last but not least, to characterize the throughput per user, we need to calculate the average number of users per BS. Finally, we derive the SINR coverage probability and spectral efficiency for both the conventional and virtualized network architectures.

III. PERFORMANCE ANALYSIS

We first characterize the association probabilities and service distances. We then calculate the average BS load per tier. We also obtain mathematical expressions for the average coverage probability and per user throughput. Note that the association probabilities, the service distances, and the BS load depend on the bias factor B, but are independent of the network architecture (i.e., conventional or virtualized). On the other hand, the coverage probabilities and throughput depend on both the bias factor and the network architecture.

[2]After C-plane splitting, not all the legacy control signaling (e.g., cell specific reference signals) are transmitted by the MBS, hence, the control burden is reduced by a factor of γ (see [4] for details).

A. Service Distances and Association Probabilities

Based on the aforementioned system model, the association probability of a typical mobile user to the disjoint sets $\mathcal{U}_1$, $\mathcal{U}_2$, and $\mathcal{U}_B$ can be characterized by the following lemma.

Lemma 1 (Association probabilities): The association probabilities are given by:

$$\mathcal{A}_1 = 2\pi\lambda_1 \int_0^\infty r\exp\left(-\pi\left(\lambda_1 r^2 + \lambda_2\left(\frac{BP_2}{P_1}\right)^{\frac{2}{\alpha_2}} r^{\frac{2\alpha_1}{\alpha_2}}\right)\right)dr, \tag{8}$$

$$\mathcal{A}_2 = 2\pi\lambda_2 \int_0^\infty r\exp\left(-\pi\left(\lambda_2 r^2 + \lambda_1\left(\frac{P_1}{P_2}\right)^{\frac{2}{\alpha_1}} r^{\frac{2\alpha_2}{\alpha_1}}\right)\right)dr, \tag{9}$$

$$\mathcal{A}_B = 2\pi\lambda_2 \int_0^\infty r\left\{\exp\left[-\pi\left(\lambda_1\left(\left(\frac{P_1}{P_2 B}\right)^{\frac{2}{\alpha_1}} r^{\frac{2\alpha_2}{\alpha_1}} + \lambda_2 r^2\right)\right)\right] - \exp\left[-\pi\left(\lambda_1\left(\left(\frac{P_1}{P_2}\right)^{\frac{2}{\alpha_1}} r^{\frac{2\alpha_2}{\alpha_1}} + \lambda_2 r^2\right)\right)\right]\right\}dr. \tag{10}$$

Proof See Appendix A.

For equal path-loss exponents ($\alpha_1 = \alpha_2 = \alpha$), the association probabilities reduce to:

$$\mathcal{A}_1 = \frac{\lambda_1}{\lambda_1 + \lambda_2\left(\frac{P_2 B}{P_1}\right)^{2/\alpha}}, \mathcal{A}_2 = \frac{\lambda_2}{\lambda_1\left(\frac{P_1}{P_2}\right)^{2/\alpha} + \lambda_2},$$

$$\mathcal{A}_B = \frac{\lambda_2}{\lambda_1\left(\frac{P_1}{P_2 B}\right)^{\frac{2}{\alpha}} + \lambda_2} - \frac{\lambda_2}{\lambda_1\left(\frac{P_1}{P_2}\right)^{\frac{2}{\alpha}} + \lambda_2}. \tag{11}$$

Conditioned on the association, we derive the probability density functions (*pdf*s) of the distances between mobile users and their serving BSs.

Lemma 2: Let R_1, R_2, and R_B denote the distances between a macro mobile user equipment and its serving MBS, a small cell mobile user equipment and its serving SBS, and a biased mobile user equipment and its serving SBS, respectively. Then, the *pdf* of R_1 is given by

$$\mathbf{f}_{R_1}(r) = \frac{2\pi\lambda_1}{\mathcal{A}_1} r\exp\left[-\pi\left(\lambda_1 r^2 + \lambda_2\left(\frac{BP_2}{P_1}\right)^{\frac{2}{\alpha_2}} r^{\frac{2\alpha_1}{\alpha_2}}\right)\right], r \geq 0.$$

The PDF of R_2 is given by

$$\mathbf{f}_{R_2}(r) = \frac{2\pi\lambda_2}{\mathcal{A}_2} r\exp\left[-\pi\left(\lambda_2 r^2 + \lambda_1\left(\frac{P_1}{P_2}\right)^{\frac{2}{\alpha_1}} r^{\frac{2\alpha_2}{\alpha_1}}\right)\right], r \geq 0.$$

The PDF of R_B is given by

$$\mathbf{f}_{R_B}(r) = \frac{-2\pi\lambda_2}{\mathcal{A}_B} r\left[\exp\left(-\pi\left(\lambda_1\left(\frac{P_1}{P_2}\right)^{\frac{2}{\alpha_1}} r^{\frac{2\alpha_2}{\alpha_1}} + \lambda_2 r^2\right)\right) - \exp\left(-\pi\left(\lambda_1\left(\frac{P_1}{BP_2}\right)^{\frac{2}{\alpha_1}} r^{\frac{2\alpha_2}{\alpha_1}} + \lambda_2 r^2\right)\right)\right], r \geq 0$$

where $\mathcal{A}_1$, $\mathcal{A}_2$, and $\mathcal{A}_B$ are given in Lemma 1

Proof See Appendix B.

B. Traffic Loads of the Network Tiers

It is useful to determine the average traffic load per BS in order to visualize the per-user throughput rather than the throughput delivered by the BS. Following [5], we calculate the traffic load per BS for each of the association cases as follows:

$$\mathcal{N}_1 = 2\pi\lambda^{(u)} \int_0^\infty r \exp\left\{-\pi\left[\lambda_1 r^2 + \lambda_2 \left(\frac{P_2 B}{P_1}\right)^{\frac{2}{\alpha_2}} r^{\frac{2\alpha_1}{\alpha_2}}\right]\right\}dr,$$
(12)

$$\mathcal{N}_2 = 2\pi\lambda^{(u)} \int_0^\infty r \exp\left\{-\pi\left[\lambda_1 \left(\frac{P_1}{P_2}\right)^{\frac{2}{\alpha_1}} r^{\frac{2\alpha_2}{\alpha_1}} + \lambda_2 r^2\right]\right\}dr,$$
(13)

$$\mathcal{N}_B = 2\pi\lambda^{(u)} \int_0^\infty r \left[\exp\left(-\pi\left(\lambda_1 \left(\frac{P_1}{P_2}\right)^{\frac{2}{\alpha_1}} r^{\frac{2\alpha_2}{\alpha_1}} + \lambda_2 r^2\right)\right)\right.$$
$$\left. - \exp\left(-\pi\left(\lambda_1 \left(\frac{P_1}{BP_2}\right)^{\frac{2}{\alpha_1}} r^{\frac{2\alpha_2}{\alpha_1}} + \lambda_2 r^2\right)\right)\right].$$
(14)

If $\alpha_1 = \alpha_2 = 4$, the loads reduces to $N_1 = \frac{\lambda^{(u)}}{\lambda_1 + \lambda_2\sqrt{\frac{P_2 B}{P_1}}}$, $\mathcal{N}_2 = \frac{\lambda^{(u)}}{\lambda_1\sqrt{\frac{P_1}{P_2}}+\lambda_2}$, and $\mathcal{N}_B = \frac{\lambda^{(u)}}{\lambda_1\sqrt{\frac{P_1}{P_2 B}}+\lambda_2} - \frac{\lambda^{(u)}}{\lambda_1\sqrt{\frac{P_1}{P_2}}+\lambda_2}$.

Note that none of the association probability, the service distance, or the load per SBS changes due to RAN virtualization. However, each MBS will be serving user plane for an average of $\mathcal{N}_1$ users and control plane for an average of $\mathcal{N}_1 + \frac{\lambda_2(\mathcal{N}_2+\mathcal{N}_B)}{\lambda_1}$ users. Furthermore, the SINR and throughput change due to the separated spectrum and control burden offload.

C. Coverage Probability and Throughput Analysis

The SINR is a very important parameter that affects many performance metrics such as the coverage probability and data rate. We characterize the SINR by deriving its complementary cumulative distribution function (*ccdf*) (i.e, $\mathbb{P}[\mathrm{SINR} > \theta]$). Without loss of generality, the SINR analysis is performed on a tagged BS located at the origin. According to Slivnyak's theorem, conditioning on having a BS at the origin does not alter the statistical properties of the coexisting Poisson point processes [16]. Therefore, the analysis holds for an arbitrary BS located at a generic location. In the case of the conventional network architecture with universal frequency reuse, the SINR of macro and small cell users is given by:

$$\mathrm{SINR}_k^{(c)} = \frac{P_k H R_k^{-\alpha_k}}{P_1 \sum_{x\in\Phi_1\backslash T_l} H_x x^{-\alpha_1} + P_2 \sum_{x\in\Phi_2\backslash T_l} H_x x^{-\alpha_2} + \sigma^2},$$
(15)

where T_l is the tagged BS (i.e, BS that serves the typical user). On the other hand, the SINR of macro and small cell users in the virtualized network architecture with dedicated spectrum access is given by:

$$\mathrm{SINR}_k^{(v)} = \frac{P_k H R^{-\alpha_k}}{P_k \sum_{x\in\Phi_k\backslash T_l} H_x x^{-\alpha_1} + \sigma^2}.$$
(16)

Due to interference management through ABS between macro cells and biased users, the SINR for both cases (i.e., conventional and virtualized) is given by:

$$\mathrm{SINR}_B^{(c)} = \mathrm{SINR}_B^{(v)} = \frac{P_2 H r^{-\alpha_2}}{P_2 \sum_{x\in\Phi_2\backslash T_l} H_x x^{-\alpha_2} + \sigma^2}.$$
(17)

The coverage probability, defined as $\mathcal{C} = \mathbb{P}[\mathrm{SINR} > \theta]$, where θ is the predefined threshold for correct signal reception, can be characterized via the following lemma.

Lemma 3: The SINR coverage for the universal frequency reuse scheme is given by

$$\mathcal{C}_1^{(c)} = \int_0^\infty \exp\left(-2\pi\lambda_1 r^2\theta^{\frac{2}{\alpha_1}} \int_{\theta^{-\frac{1}{\alpha_1}}}^\infty \frac{v}{v^{\alpha_1}+1}dv\right.$$
$$\left. -2\pi\lambda_2 r^2\theta^{\frac{2}{\alpha_2}} \left(\frac{P_2}{P_1}\right)^{\frac{2}{\alpha_2}} \int_{\left(\frac{B}{\theta}\right)^{\frac{2}{\alpha_2}}}^\infty \frac{1}{v^{\alpha_2}+1}dv\right) \mathbf{f}_{R_1}(r)dr,$$
(18)

$$\mathcal{C}_2^{(c)} = \int_0^\infty \exp\left(-2\pi\lambda_1 r^2 \left(\frac{P_1}{P_2}\right)^{\frac{2}{\alpha_1}} \theta^{\frac{2}{\alpha_1}} \int_{\theta^{\frac{1}{\alpha_1}}}^\infty \frac{v}{v^{\alpha_1}+1}dv\right.$$
$$\left. -2\pi\lambda_2 r^2\theta^{\frac{2}{\alpha_2}} \int_{\theta^{\frac{-1}{\alpha_2}}}^\infty \frac{v}{v^{\alpha_2}+1}dv\right) \mathbf{f}_{R_2}(r)dr.$$
(19)

The SINR coverage for the dedicated spectrum access scheme is given by

$$\mathcal{C}_1^{(v)} = \int_0^\infty \exp\left(-2\pi\lambda_1 r^2\theta^{\frac{2}{\alpha_1}} \int_{\theta^{-\frac{1}{\alpha_1}}}^\infty \frac{v}{v^{\alpha_1}+1}dv\right) \mathbf{f}_{R_1}(r)dr,$$
(20)

$$\mathcal{C}_2^{(v)} = \int_0^\infty \exp\left(-2\pi\lambda_2 r^2\theta^{\frac{2}{\alpha_2}} \int_{\theta^{\frac{-1}{\alpha_2}}}^\infty \frac{v}{v^{\alpha_2}+1}dv\right) \mathbf{f}_{R_2}(r)dr.$$
(21)

For biased users, the SINR coverage is given by

$$\mathcal{C}_B^{(c)} = \mathcal{C}_B^{(v)} =$$
$$\int_0^\infty \exp\left(-2\pi\lambda_2 r^2\theta^{\frac{2}{\alpha_2}} \int_{\theta^{\frac{-1}{\alpha_2}}}^\infty \frac{v}{v^{\alpha_2}+1}dv\right) \mathbf{f}_{R_B}(r)dr,$$
(22)

where $\mathbf{f}_{R_1}(r)$, $\mathbf{f}_{R_2}(r)$, and $\mathbf{f}_{R_B}(r)$ are the service distance distributions for macro, small cell, and biased users, respectively. Equations for $\mathbf{f}_{R_1}(r)$, $\mathbf{f}_{R_2}(r)$, and $\mathbf{f}_{R_B}(r)$ are given in Lemma 2

Proof See Appendix C.

For path loss exponents $\alpha_1 = \alpha_2 = 4$, the coverage probabilities reduce to the simple closed-form expressions shown below; for the universal frequency reuse, the coverage probability is given by

$$\mathcal{C}_1^{(c)} = \frac{\lambda_1 + \lambda_2\sqrt{\frac{BP_2}{P_1}}}{\lambda_1\left(1+\sqrt{\theta}\arctan\sqrt{\theta}\right) + \lambda_2\sqrt{\frac{BP_2}{P_1}}\left(1+\sqrt{\frac{\theta}{B}}\arctan\sqrt{\frac{\theta}{B}}\right)},$$
(23)

$$\mathcal{C}_2^{(c)} = \frac{\lambda_2 + \lambda_1\sqrt{\frac{P_1}{P_2}}}{\lambda_1\sqrt{\frac{P_1}{P_2}}\left(1+\sqrt{\theta}\arctan\left(\sqrt{\theta}\right)\right) + \lambda_2\left(1+\sqrt{\theta}\arctan\left(\sqrt{\theta}\right)\right)}.$$
(24)

For the dedicated spectrum access, the coverage probability is given by

$$\mathcal{C}_1^{(v)} = \frac{\lambda_1 + \lambda_2 \sqrt{\frac{BP_2}{P_1}}}{\lambda_1 \left(1 + \sqrt{\theta} \arctan \sqrt{\theta}\right)}, \quad (25)$$

$$\mathcal{C}_2^{(v)} = \frac{\lambda_2 + \lambda_1 \sqrt{\frac{P_1}{P_2}}}{\lambda_2 \left(1 + \sqrt{\theta} \arctan \left(\sqrt{\theta}\right)\right)}. \quad (26)$$

For biased users, the coverage probability is given by

$$\mathcal{C}_B^{(v)} = \mathcal{C}_B^{(c)} = \frac{-\pi\lambda_2}{\mathcal{A}_B} \left(\frac{1}{\pi\lambda_2 \sqrt{\theta} \left(\arctan\left(\sqrt{\theta}\right)\right) + \pi \left(\lambda_1 \sqrt{\frac{P_1}{P_2}} + \lambda_2\right)} \right.$$
$$\left. - \frac{1}{\pi\lambda_2 \sqrt{\theta} \left(\arctan\left(\sqrt{\theta}\right)\right) + \pi \left(\lambda_1 \sqrt{\frac{P_1}{BP_2}} + \lambda_2\right)} \right), \quad (27)$$

where $\mathcal{A}_B$ is calculated as in Eq. (11). From the coverage probability, the spectral efficiency can be derived using the following criterion

$$\mathbb{E}[\ln(1 + \text{SINR})] \overset{(a)}{=} \int_0^\infty \mathbb{P}[\ln(1 + \text{SINR}) > \zeta]d\zeta$$
$$= \int_0^\infty \mathbb{P}[\text{SINR} > (e^\zeta - 1)]d\zeta$$
$$\overset{(b)}{=} \int_0^\infty \frac{\mathbb{P}[\text{SINR} > t]}{t + 1}dt, \quad (28)$$

where (a) follows because $\ln(1 + SINR)$ is a strictly positive random variable, and (b) follows by changing variables $t = e^\zeta - 1$. Due to space limitation, we do not provide spectral efficiency equations since they can be obtained for each case by directly integrating the corresponding coverage probability, given in Lemma 3, as in shown in Eq. (28).

IV. MODEL VALIDATION AND ANALYSIS

In this section, we first validate our results using MATLAB simulations. We then use the developed analytical model to analyze the virtualized RAN performance and obtain design insights. Unless otherwise stated, the transmission powers are $P_1 = 50$ dBm, $P_2 = 5$ dBm, and the bandwidth is $W = 10$ MHz. The resource partitioning fraction is $\eta = 0.3$. The percentage of control data in the available time/frequency resources is $\mu = 0.3$ based on 3GPP Release 11 [4]. The available air interface bandwidth for macro cells resource allocation is $W_1 = 2$ MHz, and for small cells resource allocation is $W_2 = 8$ MHz. We assume that the density of MBSs is $\lambda_1 = 2$ BS/km^2 and the density of mobile users is $\lambda^u = 50$ users/km^2 The path loss exponent is $\alpha_1 = \alpha_2 = 4$.

We validate the developed analytical model by comparing the coverage probability $\mathcal{C}$ obtained from Eq. (18) to (22) with Monte Carlo simulations. Fig. 2 shows the coverage probabilities obtained through simulation and mathematical analysis for macro cell users, small cell users, and biased users
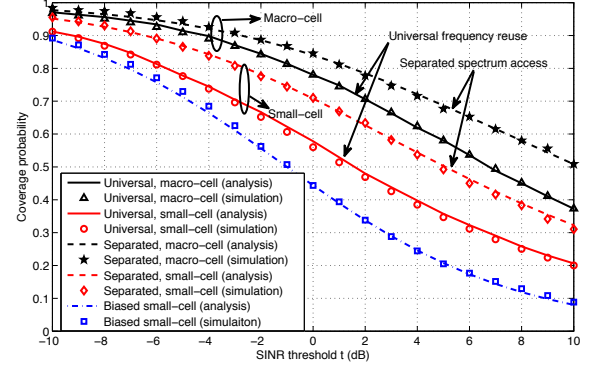

Fig. 2. Coverage probability vs the SINR threshold (θ).

for universal frequency reuse and dedicated spectrum access. The graph shows that the proposed model closely matches the simulation results, confirming the validity of the model. The graph also shows that, in comparison with dedicated spectrum access, universal frequency reuse degrades the SINR performance in terms of coverage probability due to cross tier interference. As mentioned earlier, biased users are not affected by the frequency allocation scheme due to interference coordination via ABS. Since virtualized RAN necessitates a detected spectrum access, virtualization improves the coverage probability when compared to the conventional network architecture.

Based on the equations presented in sections II-B, III-A and III-B, Fig. 3 shows the average per-user throughput, defined as $\sum_{i \in \{1,2,B\}} \mathcal{A}_i \mathcal{T}_i / \mathcal{N}_i$, as a function of small cell density for three cases: (a) virtualized RAN with $\gamma = 1$, 3, and 5, (b) conventional RAN with universal frequency reuse and (c) conventional RAN with dedicated spectrum access. The figure shows that the virtualized network architecture always outperforms the conventional network architecture with dedicated spectrum access in terms of throughput. This indicates that virtualization with dual MBS and SBS improves spectrum utilization. The figure also shows that control signaling reduction is crucial to outperform the universal frequency reuse scheme in terms of throughput. For instance, for $\gamma = 3$ and 5 network virtualization outperforms conventional network architecture with universal frequency reuse in terms of throughput.

Looking into Figs. 2 and 3 we conclude the following; in comparison with universal frequency reuse, the dedicated spectrum access scheme without virtualization offers better SINR performance (Fig. 2) at the expense of lower throughput (Fig. 3). The reason is that the data rate is given by $W \ln(1 + \text{SINR})$; hence the improvement in W dominates the improvement in SINR. The virtualized RAN with dual MBS and SBS connectivity balances the tradeoff between
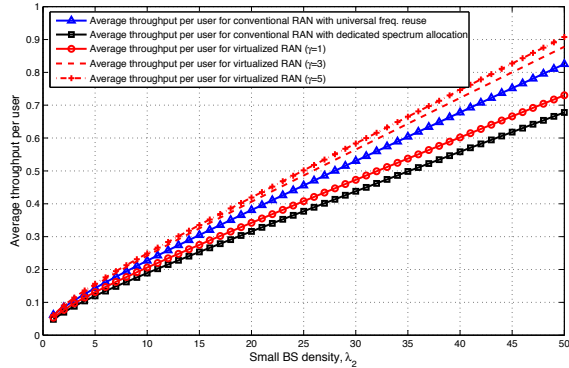
Fig. 3. Average throughput per user for universal frequency reuse and separated spectrum access.
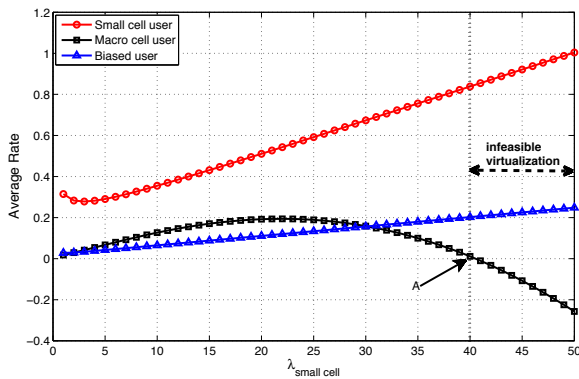

Fig. 4. Average per-user throughput vs. small cell density in virtualized network architecture (γ=3).

SINR coverage probability and throughput thanks to intelligent spectrum utilization, control signaling reduction and offloading to the macro tier. Hence, with the proper reduction of the control signaling, the virtualized network architecture outperforms both conventional schemes.

Finally, we investigate the feasibility of RAN virtualization using Fig. 4. In this figure, we plot the graphs of the average per-user throughput as a function of small cell density using Eq. (5), (6), and (7) in which the spectral efficiencies are calculated using Eq. (28). For these graphs, we assume saturation conditions such that the added SBS always have users to serve. Hence, increasing the small BSs density overloads the macro BS with large signaling overhead to deliver. Due to the limited capacity of the macro cell, there is a point (point A in Fig. 4) where the required control signaling becomes overwhelming such that the MBS cannot support. That is, the required control signaling is more than the data rate that MBS can support. At this point, RAN virtualization can only be achieved by allocating more spectrum to the MBSs in order to support the

overwhelming control load.

Another interesting observation from Fig. 4 is that the per user throughput of the macro users increases with the SBS intensity then decreases again (see "Macro cell user" curve). This behavior can be explained by the trade-off between users traffic offloading from and control offloading to the MBS. That is, by increasing the SBS density, the association probability with SBS increases, and hence, the average number of users per macro cell decreases. Hence, each macro user takes a larger portion of the available spectrum, which improves their throughput. In other words, the amount of traffic offloaded from the MBS dominates the amount of signaling offloaded to it. After a critical SBS density, the amount of control signaling offloaded to the MBS dominates the amount of traffic offloaded from it, which degrades the macro users throughput.

V. CONCLUSION

We have presented a novel analytical paradigm for virtualized radio access networks (RAN) with flexible user association. We derive simple mathematical expressions for coverage probability and throughput, which reduce to closed form in special cases. The analysis takes into account the control signaling burden, spectrum allocation schemes, and interference coordination via almost blank subframes. We then use the developed model to study RAN virtualization and quantify the performance gains obtained via control and data splitting. Finally, we discuss the feasibility of RAN virtualization in terms of the system parameters. In the future, we will investigate the impact of handover on the control signaling using RAN virtualization.

APPENDIX A
PROOF OF LEMMA 1

The association probability depends on the relative distances between the test user and the nearest BS in each tier. According to the PPP assumption, it can be shown that the *pdf* of distance between a generic user and the nearest BS from tier k is given by $f_{r_k}(r) = 2\pi\lambda_k r \exp(-\pi\lambda_k r^2)$, $0 \leq r \leq \infty$. By definition, the association probabilities can be obtained as follows:

$$\mathcal{A}_1 = \mathbb{P}\left(P_1 r_1^{-\alpha_1} > P_2 B r_2^{-\alpha_2}\right)$$
$$= \int_{r>0}\left(1 - F_{r_2}\left(\left(\frac{P_2 B}{P_1}\right)^{\frac{1}{\alpha_2}} r^{\frac{\alpha_1}{\alpha_2}}\right)\right) f_{r_1}(r)\mathrm{d}r$$
$$= \int_0^\infty \exp\left(-\pi\lambda_2\left(\frac{P_2 B}{P_1}\right)^{\frac{2}{\alpha_2}} r^{\frac{2\alpha_1}{\alpha_2}}\right) 2\pi\lambda_1 r \exp(-\pi\lambda_1 r^2)\mathrm{d}r.$$

Similarly, $\mathcal{A}_2$ and $\mathcal{A}_B$ can be obtained.

APPENDIX B
PROOF OF LEMMA 2

Association implies correlation among the relative distances between nearest BS from each tier. For instance, given that a mobile user is associated to the macro tier directly indicates that $\left(P_1 r_1^{-\alpha_1} > P_2 B r_2^{-\alpha_2}\right)$, where r_1 and r_2 are the distances to the nearest MBS and SBS, respectively. Let $f_{r_1,r_2}(x,y) =$

$f_{r_1}(x)f_{r_2}(y)$ be the joint *pdf* of r_1 and r_2, then, the *pdf* of the service distance R_1 for a macro user can be obtained as

$$f_{R_1}(x) = \frac{1}{\mathcal{A}_1} \int_{\left(\frac{P_2 B x^{\alpha_1}}{P_1}\right)^{\frac{1}{\alpha_2}}}^{\infty} f_{r_1, r_2}(x, y)dy$$

$$= \frac{1}{\mathcal{A}_1} \int_{\left(\frac{P_2 B x^{\alpha_1}}{P_1}\right)^{\frac{1}{\alpha_2}}}^{\infty} 4\pi^2 xy\lambda_1\lambda_2 \exp\left(-\pi(\lambda_1 x^2 + \lambda_2 y^2)\right) dy$$

$$= \frac{2\pi x\lambda_1}{\mathcal{A}_1}\exp\left[-\pi\left(\lambda_1 x^2 + \lambda_2\left(\frac{BP_2}{P_1}\right)^{\frac{2}{\alpha_2}} x^{\frac{2\alpha_1}{\alpha_2}}\right)\right], 0 \le x \le \infty,$$

where $\mathcal{A}_1$ is the association probability to the macro tier and is calculated in Lemma 1. Similarly, $f_{R_2}(r)$ and $f_{R_B}(r)$ are calculated.

APPENDIX C
PROOF OF LEMMA 3

Due to space constraints, we show coverage probability ($\mathcal{C}_1^{(c)}$) for a macro user in the universal frequency reuse only. The coverage probabilities in other cases ($\mathcal{C}_2^{(c)}, \mathcal{C}_B^{(c)}, \mathcal{C}_1^{(v)}, \mathcal{C}_2^{(v)}$, and $\mathcal{C}_B^{(v)}$) can be obtained using similar methodology.

Exploiting the exponential channel gains, the *ccdf* of SINR can be expressed in terms of the Laplace transform of the aggregate interference as [2], [11]:

$$\mathbb{P}[\text{SINR}_k^{(c)} > \theta] = \int_0^{\infty} \exp\left(\frac{-\sigma^2\theta r^{\alpha}}{P_1}\right) \mathcal{L}_{I_{agg}}\left(\frac{\theta r^{\alpha}}{P_1}\right) f_{R_1}(r), \tag{29}$$

where $\mathcal{L}_{I_{agg}}(s)$ is the Laplace transform (LT) of the PDF of the aggregate interference. Due to the universal frequency reuse, the aggregate interference in coming from multi-tiers $I_{agg} = \sum_k I_k$, then the LT is given by $\mathcal{L}_{I_{agg}}(s) = \prod_k \mathcal{L}_{I_k}(s)$. The LT of intra-tier interference I_1 is obtained as:

$$\mathcal{L}_{I_1}(s) = \mathbb{E}\left[e^{-s\{I_1\}}\right]$$

$$= \mathbb{E}\left[e^{-sP_1 \sum_{x \in \Phi_1 \setminus T_l} H_x x^{-\alpha_1}}\right]$$

$$= \mathbb{E}_{\phi_1}\left[\prod_{x \in \Phi_1 \setminus T_l} \mathbb{E}_H\left[e^{-sP_1 H_x x^{-\alpha_1}}\right]\right]$$

$$\overset{(e)}{=} \exp\left(-2\pi\lambda_1 \int_r^{\infty} \frac{sP_1 x^{-\alpha_1}}{1 + sP_1 x^{-\alpha_1}} x dx\right), \tag{30}$$

where (e) follows by using the Probability Generation Functional for the PPP and the LT for the exponential distribution. Note that the integration boundary r is due to the fact that the serving MBS is the nearest to the test user in the macro tier. Similarly, the LT of inter-tier interference I_2 is obtained as:

$$\mathcal{L}_{I_2}(s) = \exp\left(-2\pi\lambda_2 \int_{r^{\frac{\alpha_1}{\alpha_2}}\left(\frac{P_2 B}{P_1}\right)^{\frac{1}{\alpha_2}}}^{\infty} \frac{sP_2 x^{-\alpha_2}}{1 + sP_2 x^{-\alpha_2}} x dx\right), \tag{31}$$

where the integration boundary $r^{\frac{\alpha_1}{\alpha_2}}\left(\frac{P_2 B}{P_1}\right)^{\frac{1}{\alpha_2}}$ is a direct consequence from the association criterion. Substituting (30) and (31) in (29) and after some manipulation (18) is obtained.

REFERENCES

[1] "More than 50 billion connected devices," *Ericsson White Paper*, February 2011.

[2] H. S. Dhillon, R. K. Ganti, F. Baccelli, and J. G. Andrews, "Modeling and analysis of k-tier downlink heterogeneous cellular networks," *IEEE Journal on Selected Areas in Communications*, vol. 30, no. 3, pp. 550–560, April 2012.

[3] H. Ishii, Y. Kishiyama, and H. Takahashi, "A novel architecture for LTE-B: C-plane/U-plane split and Phantom Cell concept," in *IEEE Globecom Workshops (GC Wkshps)*, Anaheim, CA, USA, Dec. 2012, pp. 624–630.

[4] C. Hoymann, D. Larsson, H. Koorapaty, and J.-F. Cheng, "A lean carrier for LTE," *IEEE Communications Magazine*, vol. 51, no. 2, pp. 74–80, 2013.

[5] S. Singh and J. Andrews, "Joint resource partitioning and offloading in heterogeneous cellular networks," *IEEE Transaction Wireless Communication*, vol. 13, pp. 888–901, 2013.

[6] H.-S. Jo, Y. J. Sang, P. Xia, and J. G. Andrews, "Outage probability for heterogeneous cellular networks with biased cell association," in *IEEE Global Telecommunications Conference (GLOBECOM 2011)*, Houston, Texas, USA, Dec. 2011, pp. 1–5, 2011.

[7] ——, "Heterogeneous cellular networks with flexible cell association: A comprehensive downlink SINR analysis," *IEEE Transactions on Wireless Communications*, vol. 11, no. 10, pp. 3484–3495, 2012.

[8] H. ElSawy and E. Hossain, "On stochastic geometry modeling of cellular uplink transmission with truncated channel inversion power control," *IEEE Transactions on Wireless Communications*, vol. 13, no. 8, pp. 4454–4469, August 2014.

[9] H. S. Dhillon, T. D. Novlan, and J. G. Andrews, "Coverage probability of uplink cellular networks," in *IEEE Global Communications Conference (GLOBECOM)*, Anaheim, California, USA, 2012, pp. 2179–2184.

[10] M. Di Renzo, C. Merola, A. Guidotti, F. Santucci, and G. E. Corazza, "Error performance of multi-antenna receivers in a Poisson field of interferers: A stochastic geometry approach," *IEEE Transactions on Communications*, vol. 61, no. 5, pp. 2025–2047, 2013.

[11] H. ElSawy, E. Hossain, and M. Haenggi, "Stochastic geometry for modeling, analysis, and design of multi-tier and cognitive cellular wireless networks: A survey," *IEEE Communications Surveys & Tutorials*, vol. 15, no. 3, pp. 996–1019, 2013.

[12] D. Cao, S. Zhou, and Z. Niu, "Optimal base station density for energy-efficient heterogeneous cellular networks," in *IEEE International Conference on Communications (ICC)*, 2012, pp. 4379–4383.

[13] Z.-S. Syu and C.-H. Lee, "Spatial constraints of device-to-device communications," in *First International Black Sea Conference on Communications and Networking (BlackSeaCom)*, 2013, pp. 94–98.

[14] X. Lin, J. G. Andrews, and A. Ghosh, "Spectrum sharing for device-to-device communication in cellular networks," *arXiv preprint arXiv:1305.4219*, 2013.

[15] T. Bai and R. W. Heath Jr, "Coverage and rate analysis for millimeter wave cellular networks," *arXiv preprint arXiv:1402.6430*, 2014.

[16] M. Haenggi and R. K. Ganti, *Interference in Large Wireless Networks*. Now Publishers Inc, 2009.